Atomistic structure and collective dynamics in liquid Pb along the melting line up to 70 GPa: A first-principles molecular dynamics study

Taras Bryk,[1,2] Taras Demchuk,[1] and Noël Jakse[3]

[1]*Institute for Condensed Matter Physics of the National Academy of Sciences of Ukraine, 1 Svientsitskii Street, UA-79011 Lviv, Ukraine*

[2]*Lviv Polytechnic National University, UA-79013 Lviv, Ukraine*

[3]*Univ. Grenoble Alpes, CNRS, Grenoble INP, SIMaP, F-38000 Grenoble, France*

(Received 25 July 2018; published 2 January 2019)

Ab initio molecular dynamics simulations were performed to analyze changes in the structure and dynamics of molten Pb along the melting line for pressures ranging from ambient to 70 GPa. Common neighbor analysis reveals a local structural order of the underlying crystalline phase at the corresponding pressure, which increasingly competes with the existing icosahedral local order with pressure. Obtained dispersions of longitudinal and transverse collective excitations contain two branches of transverse modes for all pressures. Analysis of the pressure dependence of observed two-peak structure of the Fourier spectra of velocity autocorrelation functions allowed us to identify their peak locations with the frequencies of nonpropagating transverse branches in the second pseudo-Brillouin zone.

DOI: 10.1103/PhysRevB.99.014201

I. INTRODUCTION

Solid metals show unique properties under high pressures, which are determined by specific behavior of electron subsystem. A novel mechanism of the pressure-induced metal-nonmetal transition due to interstitial localization of electrons was predicted by Rousseau and Ashcroft [1], and proved later in experimental observations of metal-nonmetal transition in solid Li [2] and Na [3] at pressures ∼70 and 200 GPa, respectively. This initiated intensive studies of solid alkali metals under high pressure by simulations and experiments [4–7].

Much less is known about structure and dynamics of metallic melts under high pressure. Melting lines of Li, Na, K contain regions with the negative slope, i.e., $dT_m/dP < 0$, and therefore it was expected to observe some specific features of the structure and dynamics in these metallic melts. Indeed, for liquid Li was reported an exotic tetrahedral clustering at very high pressures of ∼150 GPa [8,9], which was explained to be due to the lowering of $2p$ states below the Fermi level. For liquid Na there was reported a tendency to the metal-nonmetal transition [10] at pressures above 60 GPa. For the case of liquid Rb there was simulation [11] and experimental [12] evidence of a structural transition at $T = 573$ K and pressures ∼10–12 GPa, which was explained by partial filling of the $4d$ electronic band with increasing pressure and consequently the emergence of local structures with significantly fewer nearest neighbors than is the case for low pressures.

Collective dynamics of metallic melts at high pressures revealed exotic features, too. In liquid Li at $T = 1000$ K, it was observed in *ab initio* molecular dynamics simulations (AIMD) a pressure-induced emergence of unusual high-frequency transverse collective modes [13], the frequency of which was higher than the even "bare" (undamped) frequencies of regular shear waves. Consequently, two branches of transverse excitations were reported for high pressures in liquid Li [13]. To date, there is no agreement on what kind of dynamic processes are reflected by the second high-frequency transverse branch, the existence of which was reported in many AIMD studies for different liquid metals [14–18], as well as in inelastic x-ray scattering experiments revealing transverse modes in the shape of scattering intensities [19,20]. A recent AIMD study of liquid Al, Ni, and Tl at ambient pressure [21] provided evidence for Tl that even at ambient pressure two branches of transverse modes can be observed. Another important finding reported in Ref. [21] is that the unusual high-frequency branch of transverse modes is observed in the dispersion of collective excitations simultaneously with the existing high-frequency peak appearing in the frequency spectrum of velocity autocorrelation function. The latter is absent when the high-frequency transverse branch is not observed. Recently, the emergence of the second branch in transverse dispersion was proposed to explain by nonlocal mode-coupling effects [18] which cause longitudinal-transverse (L-T) coupling outside the hydrodynamic region. Very recently there appeared a theoretical description of the L-T mixing within the generalized Born approximation [22]. The L-T coupling is known to exist in molecular liquids and in particular in water as was shown by classical [23] and *ab initio* [24] simulations as well as by scattering experiments [25].

Polyvalent liquid metal Pb was studied intensively at ambient conditions [26–30]; however, at high pressures there is presently no study of the collective dynamics by *ab initio* simulations to the best of our knowledge. The experimentally established phase diagram has a melting line increasing monotonically in the experimentally studied pressure range up to 80 GPa [31]. There is no negative-slope part of the melting curve as it is for Li, Na, K, Ga, Si, Ge, etc., whereas there exist well-established boundaries fcc to hcp to bcc crystal phases with increasing pressure. Our main aim in this study is to follow by means of AIMD simulations the increase of

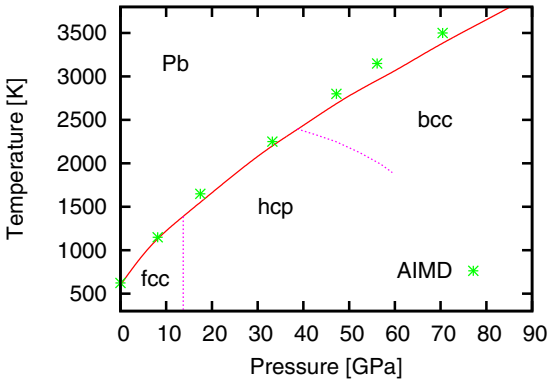

FIG. 1. Phase diagram of Pb taken from Ref. [31] (lines) and thermodynamic points simulated in this study (asterisks).

pressure along the melting line of Pb in order to estimate the effect of pressure on dispersion of longitudinal and transverse collective excitations close to melting and to establish a correlation between the structure, single-particle, and collective dynamics. There were several reports on *ab initio* studies on the structure, dynamics, and transport properties of liquid Pb, mainly at the ambient pressure [32–34], therefore we will focus on the pressure-induced changes in the structure and dynamics of liquid Pb. The remaining part of the paper is organized as follows: the next section provides details of AIMD simulations and our methodology of dispersion calculations. In Sec. III we present changes in atomistic structure along the melting curve and a common-neighbor analysis (CNA) [35] at different pressures, and we search for correlation in features of the single-particle spectra of velocity autocorrelation functions with the dispersions of L and T collective excitations at different pressures. The conclusions of this study are given in the last section.

II. SIMULATION BACKGROUND

We simulated liquid Pb at seven thermodynamic points along the experimental melting line [31] at the temperatures 623, 1150, 1650, 2250, 2800, 3150, and 3500 K, shown in Fig. 1. They correspond respectively to pressures 0, 8.2, 17.5, 33, 47.2, 56.1, and 70.5 GPa. The thermodynamic points were chosen in such a way, that at least two points were simulated for pressures corresponding different underlying solid phases, which change with the increase of pressure as fcc-hcp-bcc up to the highest studied pressure of 70.5 GPa. The corresponding number densities for the seven thermodynamic points for increasing temperature are 0.03094, 0.03407, 0.03781, 0.04374, 0.04566, 0.04738, and 0.04993 Å^{-3}. The *ab initio* simulations were performed with 300 particles in a cubic box subject to periodic boundary conditions in an NVT ensemble, and the electron-ion interaction was represented by projector augmented wave (PAW) potentials [36,37], which allow correct recovering of nodal structure of valence wave functions in core region in contrast to the standard norm-conserving pseudopotentials. For the lowest ambient pressure we used for exchange correlation the local density approximation (LDA) [38,39], while for higher pressures because of increasing nonuniform electron-density distribution the generalized gradient approximation (GGA) in the Perdew, Burke, and Ernzerhof (PBE) [40] formulation was applied. It has been demonstrated [41] that the GGA gives a good representation of the equation of state for Pb at high pressure up to 100 GPa. It is known that at ambient pressure the PBE-GGA approximation leads to overstructuring effects [21,42]. We performed a test with LDA- and PBE-GGA-derived static structure factor $S(k)$ for our lowest temperature and found approximately 15% higher amplitude of the first peak with GGA while LDA provided good agreement with the experimental data, as shown in the next section. Therefore we applied the LDA to the production runs for static and dynamic properties at the smallest studied pressure. The cutoff energy in plane-wave expansion was taken as the default one for this type of Pb-PAW potentials; namely, 98 eV. We performed a test taking the cutoff energy of 120 eV for the system at the highest studied pressure and observed a very small shift, less than one percent, in average pressure with respect to the system simulated with the default cutoff energy, making sure that the standard cutoff leads to practically converged values of the pressure. Only the Γ point was used for sampling of the Brillouin zone, which is justified by the quite large size of the disordered system. The time step for solving the equation of motions was 2 fs, which allowed us to converge the electronic contribution to the total energy within four-to-five iterations. At each time step we dumped the positions, velocities of particles, and corresponding forces, which were needed for the subsequent calculations of different time correlation functions. The production runs for each temperature were at least 24 000 time steps (for the most dense system it was 28 000 time steps) during which structural and dynamic properties were collected and analyzed in a standard way. The large number of configurations allowed us to reach a nice convergence of the tails of density-density and current-current time correlation functions, which allowed us to obtain quite smooth time-Fourier transforms.

It is, however, worth mentioning here some specific features. First, concerning the common-neighbor analysis, we have extracted 10 configurations to produce their inherent structures (IS) by bringing the system to the local minimum of the potential-energy surface, using a conjugated gradient minimization in order to suppress the thermal noise. The CNA is applied to each IS which consists of identifying pairs of atoms as described in our preceding paper [43]. Second, the longitudinal and transverse current time correlation functions

$$F^{\alpha}_{JJ}(k,t) = \langle J_{\alpha}(-k,t) J_{\alpha}(k,0)\rangle, \quad \alpha = L, T,$$
$$J_{\alpha}(k,t) = \frac{1}{\sqrt{N}} \sum_{i=1,N} v_{i,\alpha}(t) e^{-i\mathbf{k}\cdot\mathbf{r}_i(t)} \qquad (1)$$

were calculated from the trajectories of particles $\mathbf{r}_i(t)$ and corresponding velocities $\mathbf{v}_i(t)$ along the trajectories for wave numbers in the range from $k_{\min}$ up to 3 Å^{-1}. Here $k_{\min} = 2\pi/L$ is the smallest accessible wave number defined by the box length L. The $k_{\min}$ increased for our simulated thermodynamic points from 0.295 Å^{-1} at 623 K to 0.346 Å^{-1} at 3500 K. The spherical average over all possible directions of wave vectors $\mathbf{k}$ corresponding to the same absolute value k was applied to all k-dependent quantities. The dispersions of L and T collective modes were obtained from the peak locations

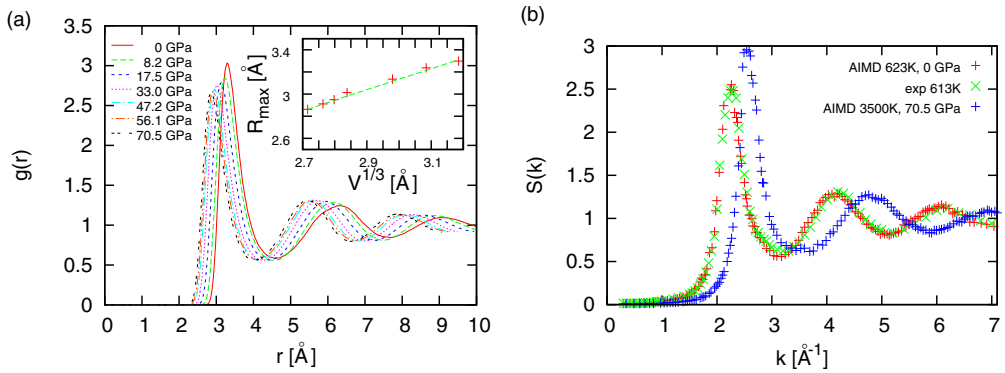

FIG. 2. (a) Pair distribution functions for liquid Pb at different thermodynamic points simulated in this study and (b) static structure factors $S(k)$, directly calculated as instantaneous density-density correlations $S(k) = \langle n(-\mathbf{k})n(\mathbf{k})\rangle$ from *ab initio* simulations at 623 K and 3500 K compared with experimental one at 613 K [44]. The inset in panel (a) shows the dependence of the first maximum location of the pair distribution functions versus cube root of atomic volume.

of L and T current spectral functions $C^L(k,\omega)$ and $C^T(k,\omega)$ which are related to the AIMD-derived current-current time correlation functions $F^L_{JJ}(k,t)$ and $F^T_{JJ}(k,t)$ via time Fourier transformation.

III. RESULTS AND DISCUSSION

A. Static structure

Atomistic structure of liquids is represented by pair distribution functions $g(r)$, which reflect the distribution of the possible distances between atomistic particles in the studied system. In Fig. 2, we show the change of calculated $g(r)$ in liquid Pb along the melting line. The right frame in Fig. 2 provides evidence of good agreement between the static structure factor $S(k)$, obtained from *ab initio* simulations at 623 K, and the available experimental one at temperature 613 K [44]. The main effect of increasing pressure on structure is the observed shift of the first peak of $g(r)$ towards smaller distances, which corresponds to more dense packing of particles and a reduction of free volume in the liquid. The inset in Fig. 2 shows that the change in atomistic structure can be represented by uniform compression model (straight line in the inset). The average number of nearest neighbors, calculated by integration of $g(r)$ until the first minimum, was monotonically increasing from 12.1 at 623 K and ambient pressure up to 13.4 at 3500 K and pressure 70.5 GPa. For structure factors we observed similar smooth changes of the shape of $S(k)$ vs pressure in shifting the first peak towards higher wave numbers and in increase of the amplitude of the first peak of $S(k)$ from 2.54 at ambient conditions to 3 at 3500 K and pressure 70.5 GPa (right frame in Fig. 2). This provides evidence that along the melting line there is no liquid-liquid transition in liquid Pb in the studied pressure range. Such structural transition has been found in liquid Rb close to the melting line at temperature 573 K in *ab initio* simulations [11] and x-ray diffraction experiments [12], and it was characterized by the reduction of the number of nearest neighbors with increasing pressure. *Ab initio* simulations enable calculations not only of atomistic structure but also of distributions of electron density around ions. In Fig. 3 we show radial electron-ion distribution functions $g_{ei}(r)$ [45] in the studied temperature-pressure range. The electron-ion distribution functions reveal the decrease of electron density in the core region that corresponds to the squeezing out of electrons into interstitial region, which in the liquid Pb however is not sufficient to trigger the emergence of new specific structural features, as was observed for liquid Li [8,9].

The smooth change of spherical-symmetric pair distribution functions $g(r)$ for liquid Pb along the melting line is in agreement with minimal changes in bond-angle (three-particle) distribution functions $P(\cos\theta)$ shown in Fig. 4. Both distribution functions, $g(r)$ and $P(\cos\theta)$, provide evidence of the absence of a liquid-liquid transition in Pb melt in the studied pressure region up to 70.5 GPa.

To reveal a correlation between the local structure of the liquid state and underlying crystalline phase at the same pressure we make use of CNA that can provide a three-dimensional view of configurations. Figure 5 displays the evolution of the bonded pairs as a function of pressure. It appears that the 15xx (sum of 1551 and 1541), associated with icosahedral ordering, are the most abundant pairs (40%) whatever the pressure and show only a modest decrease with increasing pressure. The 1431 pairs are associated with distorted icosahedra or distorted close-packed structures [46–48]. Their decrease indicates that the liquid becomes more

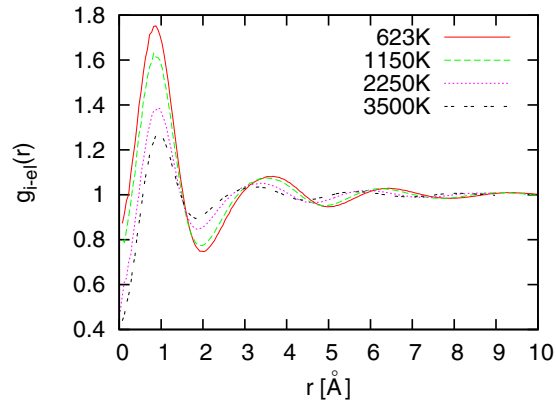

FIG. 3. Electron-ion distribution functions for liquid Pb at four thermodynamic points simulated in this study.

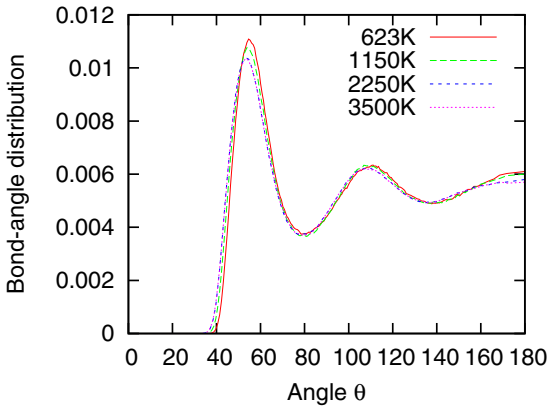

FIG. 4. Bond-angle distribution functions for liquid Pb at four thermodynamic points simulated in this study.

structured with increasing pressure. The 1421 and 1422 pairs belong to the close-packed structures such as the fcc (1421) and hcp (1421+1422) crystalline ordering. The presence of 1421 associated with the absence of 1422 at the lowest pressure is an indication of a small amount of fcc ordering (10%). At intermediated pressures, we observe a rise of the 1422 pairs indicating the change from a fcc to a hcp ordering which represents 15%. At higher pressures these two type of pairs vanish. The amount of 1441 and 1661 pairs, characteristic of the bcc crystalline order, which remain small at the lowest pressures, undergo a strong increase at 50 GPa and above. This is consistent with the evolution of the coordination number which is closer to 14, in this range of pressure. The bcc local structures, which represent nearly 50%, compete strongly with the icosahedral and defective local structures. Finally, such a result is compatible with the evolution of the phase diagram and shows that the liquid phase embodies local structural features of the underlying crystalline phase, a situation which is more significant at high pressure for the bcc ordering.

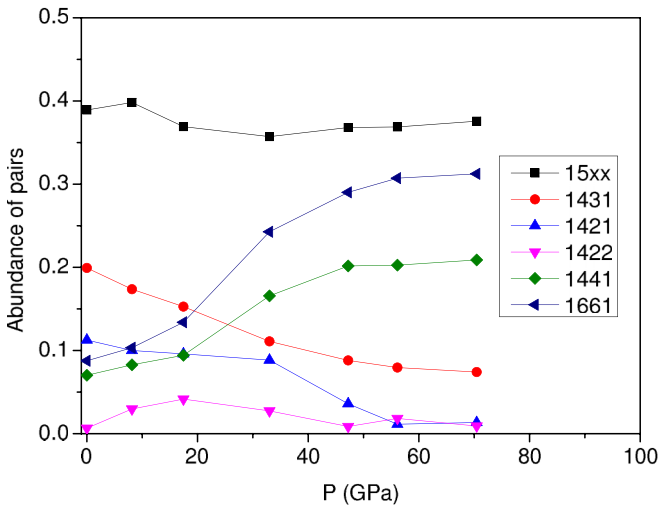

FIG. 5. Common neighbor analysis of local configurations in liquid Pb along the melting line.

B. Single-particle dynamics

The single-particle dynamics in liquids is usually studied via analysis of simulation-derived velocity autocorrelation functions (VACF) $\psi(t) = \langle \mathbf{v}_i(t)\mathbf{v}_i(0)\rangle$ and mean square displacements $R^2(t) = \langle |\mathbf{r}_i(t) - \mathbf{r}_i(0)|^2\rangle$, while another function, the single-particle density-density time correlation function $F_s(k,t)$, allows analyzing the k-dependent diffusivity from quasi-elastic neutron-scattering experiments and studying the structural relaxation times. We are interested in our study mainly in frequency spectra of velocity autocorrelation functions, because outside the low-frequency region they keep information about vibrational frequencies in the studied systems. In Fig. 6 we show the evolution of normalized velocity autocorrelation functions and their frequency spectra along the melting line. At all studied thermodynamic points the VACFs reveal oscillating behavior, which is the consequence of backscattering of particles on nearest neighbors, i.e., the cage effect. The general tendency with increasing pressure is in shifting the first negative minimum of VACF towards smaller times, which obviously is the consequence of reduction of free volume in the metallic liquid due to increase of pressure. The frequency spectra of VACF for all thermodynamic points along the melting line have clearly a two-peak shape, and with increasing pressure both peaks shift toward higher frequencies. We compare in the next section these features with the analysis of dispersion of collective excitations, i.e., the positions of maxima of VACF frequency spectra with characteristic frequencies of dispersion curves in order to establish a possible correlation.

In Fig. 7 the mean-square displacements in liquid Pb with increasing pressure along the melting line are shown. The crossover from the ballistic regime to a diffusive one shifts with the increase of pressure towards smaller times. The linear long-time behavior shifts upwards with increasing pressure, which is the consequence of the rise of diffusivity due to increase of temperature despite of reduction of free volume in liquid and the more pronounced cage effects. We observe a monotonic increase of diffusivity from 0.16 $\text{Å}^2\,\text{ps}^{-1}$ at 623 K to 0.31 $\text{Å}^2\,\text{ps}^{-1}$ at 3500 K along the melting line. Calculations of diffusivity via Kubo integrals of VACFs resulted in the same values of diffusion coefficients within 3% error bars as from the long-time asymptotes of mean square displacements. The observed monotonic dependence of the diffusivity is defined by increasing temperature for our sequence of the thermodynamic points along the melting line as well as by the absence of drastic changes in the effective atomic size for Pb for the range of pressures studied here. The latter can essentially change the monotonic pressure or temperature dependence of the diffusivity as was observed for liquid Rb [11] and liquid Na [14].

C. Pressure dependence of dispersion of collective excitations in liquid Pb along the melting line

Longitudinal collective excitations manifest as side peaks of dynamic structure factors $S(k,\omega)$, which are directly connected via convolution involving the so-called resolution function $R(\omega)$ with the experimentally measured intensity of scattered x-rays or neutrons $I(k,\omega)$. MD simulations provide a possibility to calculate directly dynamic structure factors

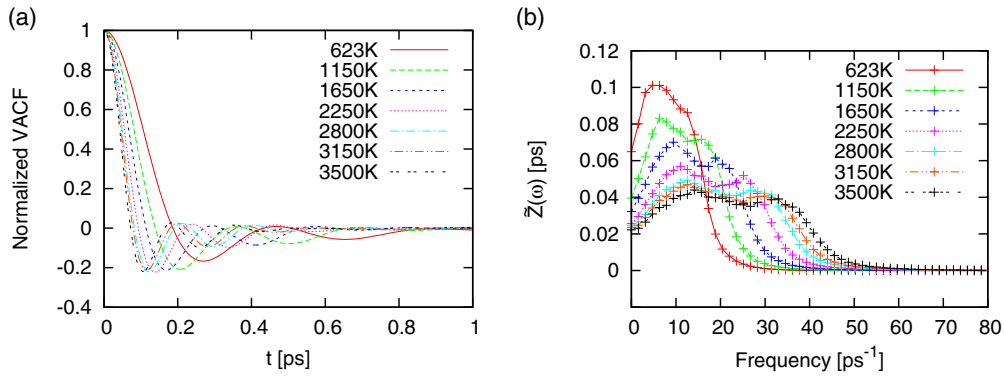

FIG. 6. (a) Normalized velocity autocorrelation functions for liquid Pb for all thermodynamic state points simulated in this study and (b) their Fourier spectra.

as well as longitudinal current spectral functions $C^L(k,\omega)$, which are related via

$$C^L(k,\omega) = \frac{\omega^2}{k^2} S(k,\omega),$$

being the consequence of the continuity equation [49,50]. We checked out the dynamic structure factors $S(k,\omega)$ in the first pseudo-Brillouin zone and found no peaks other than the acoustic Brillouin peaks. Sometimes, the fit analysis of experimental or simulation $S(k,\omega)$ can indicate a presence of contributions from nonhydrodynamic propagating modes [14,17,19,20,51]. The most correct methodology to obtain the dispersion curves of collective excitations is in separation of contributions from relaxing and propagating modes to $S(k,\omega)$ and $C^L(k,\omega)$ as this is usually performed in a parameter-free form within the generalized collective-mode (GCM) approach [52,53] or by using a fit ansatz constrained by some number of exact sum rules [54–56]. Since the heat fluctuations are extremely difficult to study within the *ab initio* simulations a new methodology was proposed in Ref. [57], which had exactly the structure of the GCM approach, however the matrix elements which involved the heat fluctuations were used as fitting parameters in a fit procedure to recover the shape of AIMD-derived time correlation functions. Transverse collective modes are much more difficult to study because in the transverse case there is no continuity equation, and consequently the transverse current spectral function $C^T(k,\omega)$ has nonzero value at zero frequency, defined by the inverse k-dependent shear viscosity $\eta^{-1}(k)$ (see Fig. 8). Starting from the ambient pressure we observed for wave numbers beyond the first pseudo-Brillouin zone the two-peak shape of the spectral functions $C^T(k,\omega)$ shown in Fig. 8. So far there is no general theory of transverse dynamics in liquids which would provide good reproduction of transverse time correlation functions outside the hydrodynamic regime (see Ref. [13]) where it is thought that there exists coupling of transverse and longitudinal dynamics. The existence of L-T coupling in liquid Pb is observed from Fig. 9, where dispersions of longitudinal and transverse excitations, obtained from maxima locations of the corresponding L and T current spectral functions are shown. Remarkably for all the studied thermodynamic state points the emergence of the second transverse branch is observed in the second pseudo-Brillouin zone. Moreover, we observed that these two branches of transverse excitations coincide with the observed high-frequency peaks on the frequency spectra of VACFs, which is consistent with our recent finding [21].

The *ab initio* simulations do not allow us to study the hydrodynamic regime of the spectra of collective excitations because of the limitations on the system size, and the expected propagation gap for transverse collective excitations at thermodynamic points close to the melting line is less than the smallest available wave numbers from AIMD. The observed almost-linear slope in the long-wavelength region of L and T dispersions is defined by the elastic high-frequency bulk B_∞

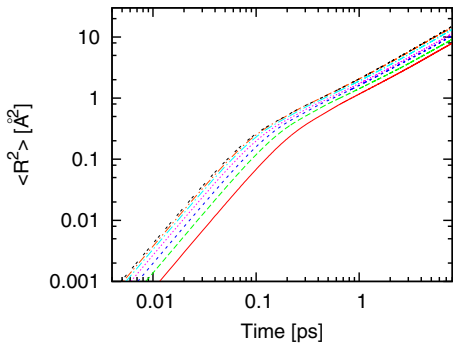

FIG. 7. Pressure dependence of the mean square displacements for liquid Pb along the melting line in log-log scale showing crossover between ballistic and diffusive regimes.

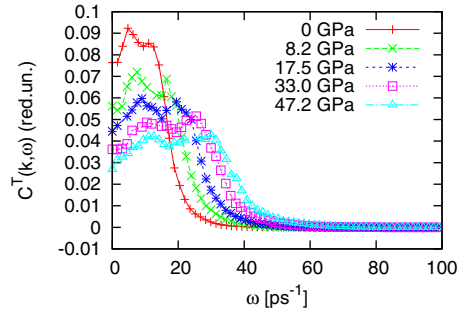

FIG. 8. Transverse current spectral functions $C^T(k,\omega)$ at close wave numbers $k \sim 2.28$–2.30 Å^{-1} for several pressures showing the two-peak frequency dependence.

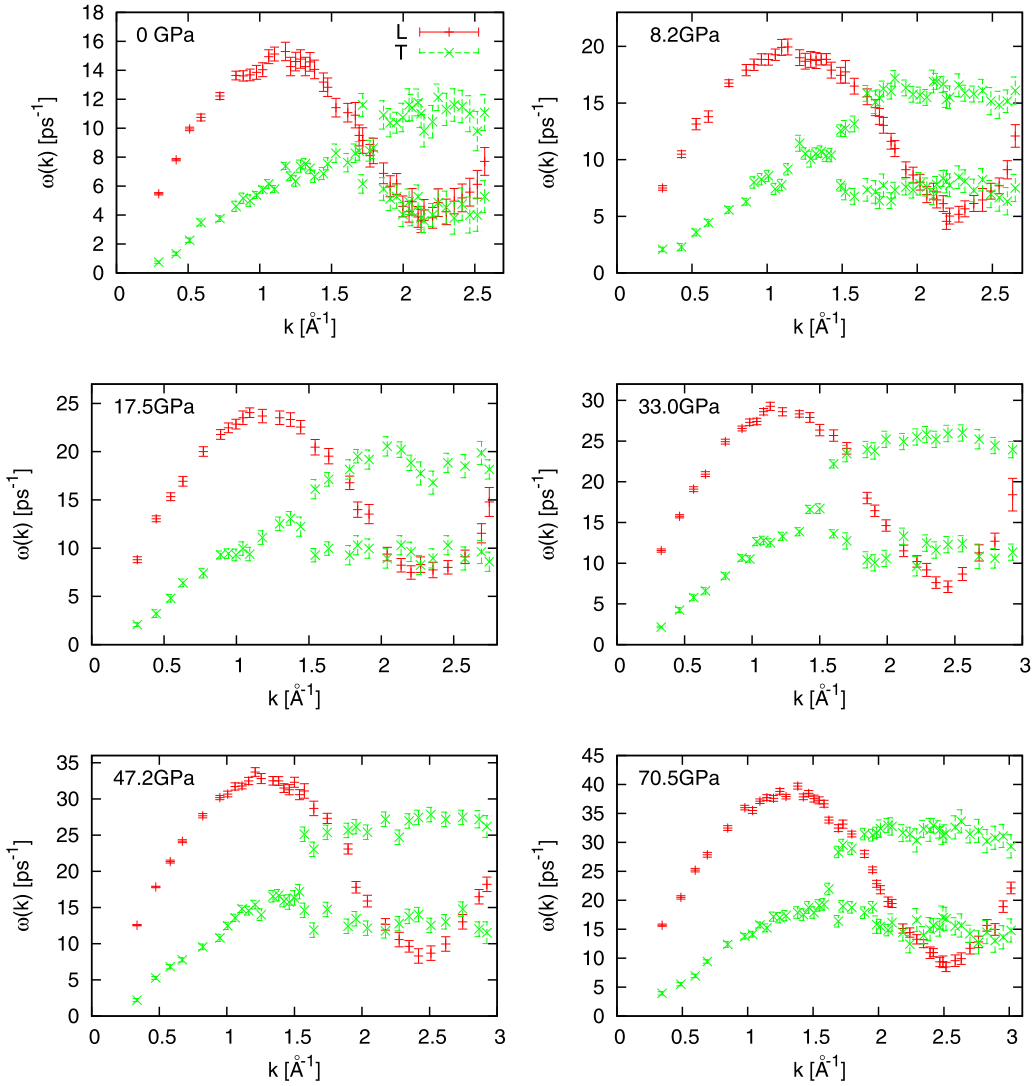

FIG. 9. Dispersion of longitudinal (L) and transverse (T) modes in liquid Pb at six thermodynamic points simulated in this study.

and shear G_∞ moduli,

$$\omega_L(k) \approx \sqrt{[B_\infty(k) + 4/3G_\infty(k)]/\rho - \sigma_L^2(k)},$$

$$\omega_T(k) \approx \sqrt{G_\infty(k)/\rho - \sigma_T^2(k)},$$

where σ_L and σ_T are the damping of L and T excitations. In Fig. 10 we show the evolution of the elastic moduli along the melting line for liquid Pb, which is almost linear with increasing pressure, which explains the observed increase of the slope of L and T dispersions in the small-k region, revealing also an increase of the sound velocities, along the melting line.

Since the maxima of vibrational spectra correspond to regions of dispersions with the zero slope we studied the pressure dependence of three characteristic frequencies in L and T dispersions: $\omega^L_{\max}$—longitudinal Debye-like frequency, which is the highest frequency in the longitudinal branch at wave numbers $k_{\max}/2$, where $k_{\max}$ corresponds to the main peak position of the static structure factor $S(k)$; two high and low transverse frequencies of practically dispersionless regions in the dispersion of T excitations in the short-wavelength region ω^T_{high} and ω^T_{low}. In Fig. 11, we show the pressure dependence of

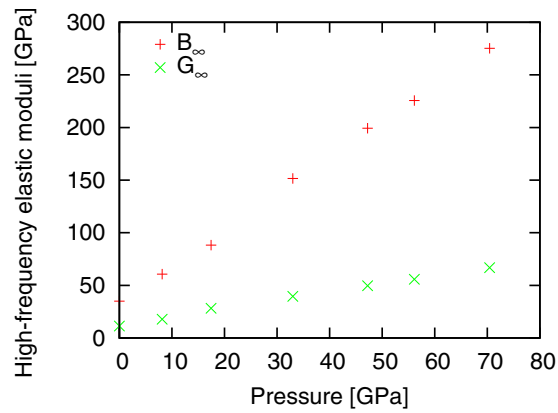

FIG. 10. Pressure dependence of the macroscopic high-frequency bulk B_∞ and shear G_∞ moduli for liquid Pb along the melting line.

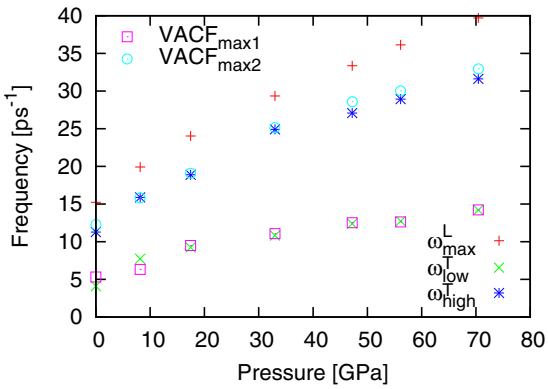

FIG. 11. Pressure dependence of the highest longitudinal frequency ω^L_{max} (Debye frequency) and high- and low-frequency transverse modes in the short-wavelength region, ω^T_{high} and ω^T_{low}.

these three characteristic frequencies along with the maxima positions of Fourier-spectra of VACFs. Figure 11 provides evidence that the frequencies of both transverse branches in the second pseudo-Brillouin zone coincide nicely with the maxima positions of the Fourier-spectra of VACFs at all pressures. Note that the modes with frequencies in the second pseudo-Brillouin zone correspond to practically single-particle vibrations in the surrounding matrix, which can be considered as an elastic medium at this timescale. Hence, VACFs as the single-particle time correlation functions reflect in their Fourier spectra short-wavelength transverse modes, which are well defined close to the melting line. Moreover, the observed two-peak structure of the Fourier-spectra of VACFs of liquid Pb along the melting line might be a consequence of oscillating transverse modes in the second pseudo-Brillouin zone. We have also to mention that another possibility of emergence of contributions from single-particle dynamics to collective spectral functions is via the mechanism of nonlocal mode coupling as was demonstrated for liquid Zn [18] and liquid Sn [58].

IV. CONCLUSION

Our *ab initio* simulations performed for seven thermodynamic points along the melting line of polyvalent metallic Pb led us to the following conclusions: (i) Although in crystalline state in the range of pressures up to 70 GPa there exist three structures changing as fcc-hcp-bcc [31], we did not find the rapid changes or any continuous structural transition in the local structure of liquid Pb slightly above the melting line in the same pressure range. (ii) A deeper analysis using the common-neighbor analysis of inherent structures of liquid Pb provides evidence that the liquid contains nearly 10% to 50% of local structural order corresponding to the underlying crystalline phase at the same pressure and increasingly competing with the 40% of existing icosahedral short-range order with pressure. (iii) The Fourier spectra of velocity autocorrelation functions for all studied pressures revealed two-peak structure because of the studied thermodynamic points were located close to the melting line and therefore had well-defined short-wavelength transverse excitations. (iv) For all the studied pressures we observed in the obtained dispersions of collective excitations two branches of transverse modes, which appear simultaneously only in the second pseudo-Brillouin zone, which can be a consequence of the coupling between short-wavelength longitudinal and transverse excitations. (v) The analysis of VACFs and dispersions of longitudinal and transverse excitations allowed us to identify frequencies of both peaks of the Fourier-transformed VACFs $\tilde{Z}(\omega)$ as coming from two flat regions of dispersions of high- and low-frequency transverse modes in the second pseudo-Brillouin zone for all the studied pressures. Our findings are in line with previous results on the analysis VACF spectra and dispersions of collective excitations in polyvalent liquid Al and Tl [21] at ambient pressure when for Ni liquid metal the high-frequency peak of $\tilde{Z}(\omega)$ and the high-frequency branch of transverse excitations were not observed. The question whether the pressure evolution of the dynamics in relation to the local structural properties found here can be similar for other metals is an important issue. Work along this line is under progress.

ACKNOWLEDGMENTS

The calculations have been performed using the *ab initio* total-energy and molecular dynamics program VASP (Vienna *ab initio* simulation program) developed at the Institute für Materialphysik of the Universität Wien [59–61]. We acknowledge the CINES and IDRIS under Project N INP2227/72914 as well as CIMENT/GRICAD for computational resources. This work was performed within the framework of the Centre of Excellence of Multifunctional Architectured Materials "CEMAM" ANR-10-LABX-44-01 funded by the "Investments for the Future" Program.

[1] B. Rousseau and N. W. Ashcroft, Phys. Rev. Lett. **101**, 046407 (2008).
[2] T. Matsuoka and K. Shimizu, Nature (London) **458**, 186 (2009).
[3] Y. Ma, M. Eremets, A. R. Oganov, Y. Xie, I. Trojan, S. Medvedev, A. O. Lyakhov, M. Valle, and V. Prakapenka, Nature (London) **458**, 182 (2009).
[4] E. Gregoryanz, L. F. Lundegaard, M. I. McMahon, C. Guillaume, R. J. Nelmes, and M. Mezouar, Science **320**, 1054 (2008).
[5] A. Lazicki *et al.*, Proc. Natl. Acad. Sci. U. S. A. **106**, 6525 (2009).
[6] M. Marques, G. J. Ackland, L. F. Lundegaard, G. Stinton, R. J. Nelmes, M. I. McMahon, and J. Contreras-Garcia, Phys. Rev. Lett. **103**, 115501 (2009).
[7] M. Marques, M. I. McMahon, E. Gregoryanz, M. Hanfland, C. L. Guillaume, C. J. Pickard, G. J. Ackland, and R. J. Nelmes, Phys. Rev. Lett. **106**, 095502 (2011).

[8] I. Tamblyn, J.-Y. Raty, and S. A. Bonev, Phys. Rev. Lett. **101**, 075703 (2008).

[9] T. Bryk, I. Klevets, G. Ruocco, T. Scopigno, and A. P. Seitsonen, Phys. Rev. B **90**, 014202 (2014).

[10] J.-Y. Raty, E. Schwegler, and S. A. Bonev, Nature (London) **449**, 448 (2007).

[11] T. Bryk, S. De Panfilis, F. A. Gorelli, E. Gregoryanz, M. Krisch, G. Ruocco, M. Santoro, T. Scopigno, and A. P. Seitsonen, Phys. Rev. Lett. **111**, 077801 (2013).

[12] F. Gorelli, T. Bryk, S. de Panfilis, L. Ulivi, G. Garbarino, and P. Parisiades, and M. Santoro, J. Phys. Chem. Lett. **9**, 2909 (2018).

[13] T. Bryk, G. Ruocco, T. Scopigno, and A. P. Seitsonen, J. Chem. Phys. **143**, 110204 (2015).

[14] M. Marqués, D. J. González, and L. E. González, Phys. Rev. B **94**, 024204 (2016).

[15] M. Marqués, L. E. González, and D. J. González, J. Phys.: Condens. Matter **28**, 075101 (2016).

[16] B. G. del Rio, O. Rodriguez, L. E. González, and D. J. González, Comput. Mater. Sci. **139**, 243 (2017).

[17] B. G. del Rio, L. E. González, and D. J. González, J. Chem. Phys. **146**, 034501 (2017).

[18] B. G. del Rio and L. E. González, Phys. Rev. B **95**, 224201 (2017).

[19] S. Hosokawa, M. Inui, Y. Kajihara, K. Matsuda, T. Ichitsubo, W.-C. Pilgrim, H. Sinn, L. E. González, D. J. González, S. Tsutsui, and A. Q. R. Baron, Phys. Rev. Lett. **102**, 105502 (2009).

[20] S. Hosokawa, S. Munejiri, M. Inui, Y. Kajihara, W.-C. Pilgrim, Y. Ohmasa, S. Tsutsui, A. Q. R. Baron, F. Shimojo, and K. Hoshino, J. Phys.: Condens. Matter **25**, 112101 (2013).

[21] T. Bryk, T. Demchuk, N. Jakse, and J.-F. Wax, Front. Phys. **6**, 6 (2018).

[22] M. G. Izzo, G. Ruocco, and S. Cazzato, Front. Phys. **6**, 108 (2018).

[23] M. Sampoli, G. Ruocco, and F. Sette, Phys. Rev. Lett. **79**, 1678 (1997).

[24] T. Bryk and A. P. Seitsonen, Condens. Matter Phys. **19**, 23604 (2016).

[25] A. Cimatoribus, S. Saccani, F. Bencivenga, A. Gessini, M. G. Izzo, and C. Masciovecchio, New J. Phys. **12**, 053008 (2010).

[26] M. Dzugutov, K.-E. Larsson, and I. Ebbsjö, Phys. Rev. A **38**, 3609 (1988).

[27] M. Dzugutov and U. Dahlborg, Phys. Rev. A **40**, 4103 (1989).

[28] W. Gudowski, M. Dzugutov, and K. E. Larsson, Phys. Rev. E **47**, 1693 (1993).

[29] T. Bryk and I. Mryglod, Phys. Rev. E **63**, 051202 (2001).

[30] T. Bryk and I. Mryglod, Phys. Rev. E **64**, 032202 (2001).

[31] A. Dewaele, M. Mezouar, N. Guignot, and P. Loubeyre, Phys. Rev. B **76**, 144106 (2007).

[32] G. Kresse, J. Non-Cryst. Solids **312-314**, 52 (2002).

[33] F. Knider, J. Hugel, and A. V. Postnikov, J. Phys.: Condens. Matter **19**, 196105 (2007).

[34] M. M. G. Alemany, R. C. Longo, L. J. Gallego, D. J. Gonzalez, L. E. Gonzalez, M. L. Tiago, and J. R. Chelikowsky, Phys. Rev. B **76**, 214203 (2007).

[35] J. D. Honeycutt and H. C. Andersen, J. Phys. Chem. **91**, 4950 (1987).

[36] P. E. Blöchl, Phys. Rev. B **50**, 17953 (1994).

[37] G. Kresse and D. Joubert, Phys. Rev. B **59**, 1758 (1999).

[38] D. M. Ceperley and B. J. Alder, Phys. Rev. Lett. **45**, 566 (1980).

[39] J. P. Perdew and A. Zunger, Phys. Rev. B **23**, 5048 (1981).

[40] J. P. Perdew, K. Burke, and M. Ernzerhof, Phys. Rev. Lett. **77**, 3865 (1996).

[41] F. Cricchio, A. B. Belonoshko, L. Burakovsky, D. L. Preston, and R. Ahuja, Phys. Rev. B **73**, 140103(R) (2006).

[42] M. Chen, H.-Y. Ko, R. C. Remsing, M. F. Calegari Andrade, B. Santra, Z. Sun, A. Selloni, R. Car, M. L. Klein, J. P. Perdew, and X. Wu, Proc. Natl. Acad. Sci. U. S. A. **114**, 10846 (2017).

[43] N. Jakse and A. Pasturel, Mod. Phys. Lett. B **20**, 655 (2006).

[44] http://res.tagen.tohoku.ac.jp/~waseda/scm/LIQ/all/pb.html.

[45] G. A. de Wijs, G. Pastore, A. Selloni, and W. van der Lugt, Phys. Rev. Lett. **75**, 4480 (1995).

[46] N. Jakse and A. Pasturel, Phys. Rev. Lett. **91**, 195501 (2003).

[47] N. Jakse, O. Le Bacq, and A. Pasturel, Phys. Rev. B **70**, 174203 (2004).

[48] N. Jakse and A. Pasturel, J. Chem. Phys. **120**, 6124 (2004).

[49] J.-P. Hansen and I. R. McDonald, *Theory of Simple Liquids*, 3rd ed. (Academic Press, London, 2006).

[50] J.-P. Boon and S. Yip, *Molecular Hydrodynamics* (McGraw-Hill, New York, 1980).

[51] T. Bryk and J.-F. Wax, J. Chem. Phys. **144**, 194501 (2016).

[52] I. M. Mryglod, I. P. Omelyan, and M. V. Tokarchuk, Mol. Phys. **84**, 235 (1995).

[53] T. Bryk, I. Mryglod, and G. Kahl, Phys. Rev. E **56**, 2903 (1997).

[54] Y. Chushak, J. Hafner, and G. Kahl, Phys. Chem. Liq. **29**, 159 (1995).

[55] Y. Chushak, T. Bryk, A. Baumketner, G. Kahl, and J. Hafner, Phys. Chem. Liq. **32**, 87 (1996).

[56] J.-F. Wax and T. Bryk, J. Phys.: Condens. Matter **25**, 325104 (2013).

[57] T. Bryk and G. Ruocco, Mol. Phys. **111**, 3457 (2013).

[58] B. G. del Rio, M. Chen, L. E. González, and E. A. Carter, J. Chem. Phys. **149**, 094504 (2018).

[59] G. Kresse and J. Hafner, Phys. Rev. B **47**, 558 (1993); **49**, 14251 (1994).

[60] G. Kresse and J. Furthmüller, Comput. Mater. Sci. **6**, 15 (1996).

[61] G. Kresse and J. Furthmüller, Phys. Rev. B **54**, 11169 (1996).